Available online at www.sciencedirect.com

ScienceDirect

journal homepage: www.intl.elsevierhealth.com/journals/dema

Effect of titania addition and sintering temperature on the microstructure, optical, mechanical and biological properties of the Y-TZP/TiO_2 composite

Ranulfo Benedito de Paula Miranda[a], *Tayná Paula Leite*[b], *Ana Clara Fagundes Pedroni*[b], *Márcia Martins Marques*[a], *Nelson Batista de Lima*[c], *Juliana Marchi*[d], *Paulo Francisco Cesar*[b,*]

[a] *Programa de Pós-Graduação em Odontologia, Universidade Ibirapuera, São Paulo, SP, Brazil*
[b] *Departamento de Biomateriais e Biologia Oral, Faculdade de Odontologia, Universidade de São Paulo, São Paulo, SP, Brazil*
[c] *Centro de Ciência e Tecnologia de Materiais, Instituto de Pesquisas Energéticas e Nucleares, São Paulo, SP, Brazil*
[d] *Centro de Ciências Naturais e Humanas, Universidade Federal do ABC, Santo André, SP, Brazil*

ARTICLE INFO

Keywords:
Dental implants
Y-TZP
Titania
Sintering temperature
Biological behavior
Optical properties
Mechanical properties

ABSTRACT

Objective. The aims of this study were: 1) to evaluate the effect of sintering temperature on microstructure, density and flexural strength of a 3Y-TZP/TiO_2 composite containing 12.5 wt% of TiO_2 compared to 3Y-TZP specimens (control); 2) to compare 3Y-TZP with the experimental 3Y-TZP/TiO_2 composite, both sintered at 1400 °C, with respect to the following parameters: optical properties, characteristic strength, Weibull modulus, fatigue behavior, induction of osteoblasts proliferation and differentiation (mineralization nodules formation).

Methods. The 3Y-TZP and 3Y-TZP/TiO_2 powders were uniaxially pressed and sintered at 1200 °C, 1300 °C, 1400 °C or 1500 °C for one hour in a furnace. The microstructural analysis consisted of X-ray diffraction and scanning electron microscopy. The density was measured by the Archimedes' principle and the flexural strength was obtained by the biaxial flexure test. The optical properties were measured using a spectrophotometer operating in the visible light wavelength range. The step-stress accelerated life testing was performed by the pneumatic mechanical cycler and the biological behavior achieved by using osteoblast-like cells (Osteo-1 cell line).

Results. Tetragonal zirconia was identified in all groups and cubic zirconia was identified only at 3Y-TZP group. The addition of TiO_2 decreased the values of density and flexural strength of the composite 3Y-TZP/TiO_2 in relation to 3Y-TZP regardless of the sintering temperature. The color difference between the two materials was not significant regarding L*a*b* parameters. The composite showed higher probability of failure, and induced higher proliferation and differentiation than control.

* *Corresponding author at:* Departamento de Biomateriais e Biologia Oral, Faculdade de Odontologia, Universidade de São Paulo, Av. Professor Lineu Prestes, 2227, Cidade Universitária, 05508-000 São Paulo, SP, Brazil.
E-mail address: paulofc@usp.br (P.F. Cesar).

https://doi.org/10.1016/j.dental.2020.08.014

Significance. The composite developed have good aesthetic and biologics properties. However, its microstructure and mechanical properties need to be improved for future dental implant applications.

1. Introduction

The use of yttria-stabilized tetragonal zirconia polycrystal (Y-TZP) in dentistry has increased considerably in recent years. Properties, such as the whitish coloration, excellent biocompatibility and good mechanical properties, allow this ceramic to be applied in the fields of prosthodontics, orthodontics and implantology. Another factor that explains the great popularity of this material is the use of CAD-CAM technology, which facilitates the production of the zirconia restorations [1–3].

Among all dental ceramics, 3Y-TZP (3 mol% of yttria) is the only one that possesses the toughening mechanism of displacive transformation. This phenomenon occurs when stresses are concentrated around existing defects in the material, triggering the transformation of the tetragonal grains into monoclinic grains. This transformation results in a volumetric expansion and also in many inter-related phenomena associated with the transformation cone formed at the crack tip [4], that allowing 3Y-TZP to have a great ability to resist crack propagation and to exhibit higher fracture toughness compared to the veneering ceramics [5].

In implantology, the gold standard material for rehabilitation is titanium (commercially pure or titanium alloy). High mechanical properties and good biocompatibility explain the success of this material in clinical studies with long follow-up periods [6]. However, the grayish coloration of titanium is a major disadvantage in clinical rehabilitations with high esthetic demand. This situation is highly critical in the anterior dentition for patients with thin gingival biotype and with a high smile, because in these cases, blackened halos may appear near the perimplant regions. One option in these cases would be the use of 3Y-TZP implants, as their whitish shade may lead to better aesthetic results [7].

On the other hand, 3Y-TZP is considered a relatively bioinert biomaterial [8], which may impair osseointegration and increase the failure rate of the implant. To solve this problem, different ceramic composites were developed by adding to the matrix of the 3Y-TZP bioactive ceramics, such as calcium phosphates, bioactive glasses and titania [9–11]. The objective of these additions is to develop a ceramic composite that is more bioactive than 3Y-TZP and that will lead to a faster and more reliable osseointegration process.

The highly bioactive behavior of titania or titanium dioxide (TiO_2) is associated with the formation of Ti−OH groups on its surface. These groups induce the adhesion of proteins, which in turn facilitate cellular adhesion and are also related to the nucleation of calcium phosphates when immersed into a solution of ionic composition similar to blood plasma (SBF) [8,12,13]. In vitro studies associated titania with improved cell adhesion, spreading, proliferation and differentiation [14–16]. In addition, animal study showed improved bone formation around implants with the presence of titania nanotubes in comparison to implants without this superficial alteration [17].

The literature shows two different methodologies for obtaining 3Y-TZP/TiO_2 composites. One of them involves synthesis by means of the sol–gel route, using zirconium oxychloride, titanium chloride and yttrium chloride [11,18]. An alternative route involves mixing commercial powders of Y-TZP and titania in a ball mill [19]. The sol-gel methodology results in more homogeneous materials; however it has several steps and consequently is very time-consuming. On the other hand, mixing commercial powders is faster, but generally results in less homogeneous powders. Additional advantage of commercial Y-TZP powders is that they have nanometric dimensions, contain small amounts of alumina (0.5 wt%) reducing low temperature degradation of 3Y-TZP and mainly exhibits suitable sintering properties.

Many studies in the literature have shown the great potential of 3Y-TZP/TiO_2 composite to be used as a biomaterial. This type of composite favors cell growth when compared to pure 3Y-TZP and has bioactivity, as it allows the formation of calcium phosphate on its surface. However, there is no consensus in the literature regarding which titania content should be added to 3Y-TZP powders and what is the most appropriate sintering temperature to obtain the maximum density of the composite [11,20–22]. In addition, 3Y-TZP/TiO_2 composites have not been characterized yet in terms of optical properties, fatigue behavior, and biological abilities, such as cell proliferation and differentiation.

The development of a novel ceramic composite for dental implant application with high osseointegration capacity requires a broad characterization, involving analysis of the microstructure, mechanical, optical and biological properties. Therefore, the general objective of the present work was to develop the 3Y-TZP/TiO_2 composite for dental implant application. The specific objectives were: 1) to evaluate the effect of the sintering temperature (1200 °C, 1300 °C, 1400 °C and 1500 °C) on the microstructure, density, and flexural strength of 3Y-TZP specimens (control) compared to a 3Y-TZP/TiO_2 composite containing 12.5 wt% of TiO_2; 2) to compare the control (3Y-TZP) with a Y-TZP/TiO_2 composite (12.5 wt%), both sintered at 1400 °C, with respect to the following parameters: optical properties, characteristic strength (σ_o), Weibull modulus (m), fatigue behavior (probability of failure estimated under fatigue at stresses of either 50 or 100 MPa, after missions of 1, 3 or 5 million cycles), induction of osteoblast proliferation and differentiation (mineralization nodules formation). The following hypotheses were tested: a) the sintering temperature would affect the properties of both the 3Y-TZP and the 3Y-TZP/TiO_2 composite and 2) the control and the composite would have similar behavior with respect to all parameters tested.

Table 1 – Studied compositions of 3Y-TZP/TiO2 ceramic powder.

Groups	Composition (wt%)	
	3Y-TZP (Tosoh, Japan) (3 mol% of yttria)	TiO_2 (Sigma Aldrich, US)
3Y-TZP	100.0	0
T12.5	87.5	12.5

2. Materials and methods

2.1. Preparation of Y-TZP/TiO_2 composite

The starting materials chosen for this work were the commercial powders of tetragonal zirconia stabilized with 3 mol% yttria, Y-TZP (TZ-3YB-E, Tosoh, Japan) and TiO_2 (Sigma-Aldrich, US). The mixture of 3Y-TZP (87.5% by weight) and TiO_2 (12.5% by weight) was performed in a polymer flask with alumina balls and isopropyl alcohol using a ball mill for 10 h and then dried at 150 °C for six hours to evaporate the isopropyl alcohol. At the end, two compositions (Table 1) were studied: the 3Y-TZP and the 3Y-TZP/TiO_2 composite (T12.5).

2.2. Processing of specimens

The 3Y-TZP and T12.5 powders were uniaxially pressed (50 MPa) into metal matrices and sintered at 1200 °C, 1300 °C, 1400 °C or 1500 °C for one hour in a furnace (Zircar, US). The specimens (n = 5 for each group and n total = 40) had their surface rectified in a semiautomatic polishing machine (Ecomet II, Buehler, US) with a diamond disk (Dia-Grid Diamond, 120 Grit Resin Bond, 12, Allied, US). The choice of a rough surface finish is related to an approximation with the surface applied to commercial 3Y-TZP implants, which are usually milled. The final dimensions of the specimens were approximately 12 mm in diameter and 1 mm in thickness for the mechanical testing and approximately 8 mm in diameter and 1 mm in thickness for the biological analyzes.

2.3. Microstructural analysis

The microstructural analysis consisted of X-ray diffraction (XRD, Rigaku, DMAX 2000, Japan) using $CuK_\alpha 1$ radiation (step size of 0.02 degree and acquisition time of 5 s) and scanning electron microscopy (SEM, Quanta 650 FEG, FEI, US). The specimens were polished and subjected to thermal etching (50 °C below the sintering temperature for 30 min) in a furnace (Zircar, US) to reveal inter-granular boundaries. Grain size of the 3Y-TZP and T12.5 was estimated by the linear intercept method with SEM images. The chemical mapping was obtained by dispersive energy spectroscopy (EDS, Quanta 650 FEG, FEI, US).

2.4. Density and flexural strength

The final density after sintering was determined using the Archimedes' principle, with water as the immersion liquid. Theoretical density was calculated using the Rietveld refinement. For the biaxial flexural strength test, the specimens were fractured using a piston on three balls device in a universal testing machine (EMIC DL 200, Brazil). During the test, the specimens were immersed in water at 37 °C. For each group, five specimens were tested at a loading rate of 0.5 mm/min. The flexural strength was calculated according to Eq. (1) (ISO 6872/2008) [23]:

$$\sigma_f = \frac{-0,2387\,F\,(X-Y)}{b^2} \quad (1)$$

where F is the fracture load, b is the specimen thickness and X and Y were determined by Eqs. (2) and (3).

$$X = (1+\upsilon)\cdot \ln\left(\frac{B}{C}\right)^2 + \left(\frac{1-\upsilon}{2}\right)\cdot\left(\frac{B}{C}\right)^2 \quad (2)$$

$$Y = (1+\upsilon)\left[1+\ln\left(\frac{A}{C}\right)^2\right] + (1-\upsilon)\cdot\left(\frac{A}{C}\right)^2 \quad (3)$$

where υ is the Poisson's ratio (0.31 for the 3Y-TZP group and 0.32 for the T12.5 group), A is the radius of the support circle (4 mm), B is the radius of the tip of the piston (0.85 mm) and C is the radius of the specimen (~6 mm).

2.5. Optical properties and Weibull analysis

The optical properties were measured using CM 3700d spectrophotometer (Konica Minolta, Japan) operating in the wavelength (λ) range of visible light (360–740 nm, with 10 nm interval). The following parameters were standardized: observer function at 2°, illuminant D65 (daylight illuminant) and the specular component excluded were used. The specimens were placed on a white background in reflectance mode and a coupling agent was used to prevent light scattering. The color difference between the 3Y-TZP and the 3Y-TZP/TiO_2 composite was calculated using the CIEDE2000 (ΔE_{00}), using Eq. (4) [24]:

$$\Delta E_{00} = \left[\left(\frac{\Delta L'}{K_L S_L}\right)^2 + \left(\frac{\Delta C'}{K_C S_C}\right)^2 + \left(\frac{\Delta H'}{K_H S_H}\right)^2 + R_T\left(\frac{\Delta C'}{K_C S_C}\right)\left(\frac{\Delta H'}{K_H S_H}\right)\right]^{\frac{1}{2}} \quad (4)$$

where $\Delta L'$, $\Delta C'$, and $\Delta H'$ are the differences in lightness, chroma and hue between the Y-TZP group and the T12.5 group. S_L, S_C, and S_H are the weighting functions for the lightness, chroma, and hue components. K_L, K_C, K_H are the correction terms to be adjusted according the experimental conditions, in this study, they were set at 1.

For the Weibull analysis, 30 specimens were fractured for each group. The Weibull modulus (m) and the characteristic strength (σ_0) with the respective upper and lower limits of the 95% confidence intervals were calculated using the maximum probability method.

2.6. Step-stress accelerated life testing

Step-stress accelerated life testing (SSALT) consisted of subjecting the specimens to different cycling profiles. For each

profile, 10 specimens from each group were cycled immersed in water. The cycles were performed by the pneumatic mechanical cycler (Biocycle, Biopdi, Brazil) with the frequency of 2 Hz. Ïston-on-three-ballsdevices were fitted on the mechanical cycler and the specimens were positioned on the devices.

The first step was carried out with loads of 135 N, which generated tensions of approximately 170 MPa in the specimens. For the next steps, the applied load was always 25 N higher than the previous one. Loads were raised until all specimens were fractured during cycling. Three cycling profiles were used: slow, moderate, and accelerated. The difference between them consisted in the number of cycles to which the specimens were submitted until finalizing a step. This number was 21,600 cycles for the accelerated profile, 43,200 cycles for the moderate profile and 64,800 cycles for the slow profile.

The SSALT data were calculated by a power law relationship for damage accumulation. The experimental data (number of cycles and stresses accumulated for each specimen) was used to estimate the probability of failure at stresses of 50 or 100 MPa after missions of 1, 3 or 5 million cycles. These estimations were made using the software Weibull++/Alta Pro 7 (Reliasoft, Tucson, US). The Beta (β) was given by Eq. (5) [25]:

$$f(T) = \frac{\beta}{\eta}\left(\frac{T}{\eta}\right)^{\beta-1} e^{-(\frac{T}{\eta})^{\beta}} \quad (5)$$

where $f(T) \geq 0$, $T \geq 0$, $\beta > 0$, $\eta > 0$, η = scale parameter and β = shape parameter (or slope).

2.7. Biological analyzes

2.7.1. Cell culture

A cell line established by Lavos-Valareto et al. [26] from parietal bone of newborn rats (Osteo-1 cells) and characterized by Togashi et al. [27] was used for evaluating the biological properties of the of the 3Y-TZP/TiO_2 composite. This cell line has already been used for analyzing aspects of osseointegration of dental materials [27]. The cells were cultured in clonogenic DMEM culture medium (Dulbecco's modified Eagle medium high-glucose) (Gibco, US) supplemented with 10% of fetal bovine serum (Gibco) and 1% penicillin-streptomycin (Gibco). The cells were maintained in a humid 5% CO_2 incubator at 37 °C. Cell growth was followed daily under an inverted phase microscope, and the culture medium was replaced every 2 or 3 days, according to the level of cellular metabolism. All cell culture procedures were performed under a laminar flow hood, following the sterility protocols of the materials and solutions (safety standards NBR/IEC 601.2.22 and IEC 60825-1/2001-8).

2.7.2. Cell plating

For the experiments the cells (1×10^4 cells) were plated on the top of 3Y-TZP and T12.5 specimens previously placed at the bottom of wells of 24-well plates. Cells plated at plain wells were used, as controls. The effects of the ceramic materials on the Osteo-1 cells were analyzed by 1) Scanning electron microscopy for assessing morphology of adhered cells; 2) Alamar Blue cell viability assay for assessing the proliferation of cells and 3) Alizarin red assay for assessing the osteogenic functional differentiation by measuring mineralized matrix formation.

2.7.3. Adhesion and cellular morphology

For the analysis of the adhesion and morphology of the cells adhered to the ceramic materials, the specimens were processed for scanning electron microscopy (SEM) 24 h after cell plating. Briefly, the cells were washed twice in phosphate-buffered saline (PBS) and fixed in 2% glutaraldehyde solution for at least 2 h. Then, the cells were dehydrated in increasing concentration of ethanol solutions (30–100%) and hexamethyldisilizane (HMDS, Sigma-Aldrich, US). The specimens were then sputtering coated with a gold palladium alloy and visualized under a scanning electron microscope (Quanta 650 FEG, FEI, US).

The experiments of cell proliferation and formation of mineralization nodules were repeated at least three times. For these analyses three experimental groups were considered, as follows:

(1) Control-cells grown in plain culture wells;
(2) 3Y-TZP- cells grown on the top of 3Y-TZP disks;
(3) T12.5- cells grown ion the top of T12.5 disks.

2.7.4. Cell proliferation

Cells were seeded as described previously and cultured for 6 days (n = 6). The Alamar Blue cell viability assay (Invitrogen, US) was used to determine the metabolic activity of cells and thereby estimate cell proliferation over time. Briefly, AlamarBlue® reagent was added directly to each well, the plates were incubated at 37 °C to allow cells to convert resazurin to resorufin, and the fluorescence signal was measured every 24 h after plating. The fluorescence was quantified in spectrophotometer (Synergy HT, US) with excitation wavelength 535 nm and emission 590 nm. The results were expressed in relative units of fluorescence (RUF).

2.7.5. Formation of mineralization nodules

The Alizarin Red assay was used to evaluate the mineralized matrix formation after 21 days in culture (n = 4). Briefly, the cells plated at the top of the ceramic specimens, as well as those plated at the 24-well plain culture plates (control group) were cultured in clonogenic medium (no mineralized medium was used). Twenty-one days later the cells were washed with PBS and fixed with 10% formaldehyde solution for 30 min at room temperature. After rinsing with distilled water, the cells were stained with Alizarin red for 30 min. Then the dishes were washed with distilled water and allowed to dry at room temperature. The nodules were dissolved in a 10% ammonia solution, and the absorbance was quantified in spectrophotometer (Synergy HT, US) with wavelength 550 nm. The results were expressed in relative units of absorbance (RUA).

2.8. Analysis of results

Flexural strength, density and metabolic activity were analyzed by analysis of variances (ANOVA), followed by the Tukey's test. Mineralization and optical properties data were analyzed

Table 2 – Mean ± standard and deviation (coefficient of variation) of percent of theoretical density (p), flexural strength (σ_f) and grain size (gs). Values followed by the same small letter are statistically similar (p > 0.05).

Groups	Sintering temperature	Parameter		
		Percent of theoretical density (%)	Flexural strength (MPa)	Grain size (μm)
3Y-TZP	1200 °C	0,91[b] ± 0.01 (1.1%)	567.4[b] ± 35.2 (6.2%)	0.17
	1300 °C	0,97[a] ± 0.01 (0.2%)	635.4[a] ± 39.2(6.2%)	0.28
	1400 °C	0,99[a] ± 0.01 (0.8%)	705.0[a] ± 57.4 (8.1%)	0.32
	1500 °C	0,98[a] ± 0.01 (1.4%)	735.8[a] ± 108.4 (14.7%)	0.44
T12.5	1200 °C	0,53[d] ± 0.6 (2.1%)	79.8[c] ± 11.0 (13.8%)	0.16
	1300 °C	0,72[c] ± 0.6 (6.5%)	263.3[b] ± 27.9 (10.6%)	0.33
	1400 °C	0,89[b] ± 0.6 (6.5%)	430.4[a] ± 20.0 (4.6%)	0.84
	1500 °C	0,96[a] ± 0.01 (1.5%)	420.9[a] ± 26.4 (6.3%)	2.19

by the Student's t-test. The level of significance was set at 5% ($p \leq 0.05$).

3. Results

3.1. Density, flexural strength and grain size

Table 2 shows the values of density, flexural strength and grain size as a function of the material and sintering temperature. The addition of TiO_2 decreased the values of percent of theoretical density and flexural strength of the composite 3Y-TZP/TiO_2 in relation to the values obtained for the 3Y-TZP regardless of the sintering temperature. 3Y-TZP sintered at 1200 °C showed values percent of theoretical density and flexural strength significantly lower than the values obtained at other temperatures, which were statistically similar. For the composite, the increase in the sintering temperature caused a significant increase in the percent of theoretical density. With respect to the flexural strength of the composite, the sintering temperatures of 1400 °C and 1500 °C resulted in higher mean values than those obtained at lower temperatures.

3.2. Microstructure

Fig. 1 shows scanning electron micrographs of the surface of the pellets of the eight experimental groups produced. All materials obtained showed microstructure containing approximately aquiaxial grains. It was possible to observe that, except for the temperature of 1200 °C, the 3Y-TZP/TiO_2 composite always showed larger grain sizes compared to the 3Y-TZP (Fig. 1 and Table 2). In addition, for both materials studied, the increase in sintering temperature led to an increase in grain size. Fig. 1a–d shows the presence of pores for both materials when sintered at 1.200 and 1.300 °C.

The chemical mapping of the composite by EDS can be observed in Fig. 2. Two different regions are identified in these figures: a) red region, corresponding to the high concentration of the chemical element zirconium and b) blue region, corresponding to the high concentration of the titanium chemical element. Black regions, corresponding to porosities, can also be identified for all temperatures studied. The EDS analysis of the blue region (Fig. 2e) showed that the Ti peaks have higher intensity than the Zr peaks, whereas in the red region (Fig. 2f), the intensities of these peaks were inverted.

Fig. 3 shows the X-ray diffraction patterns of the sintered specimens. Peaks corresponding to the crystalline phase of tetragonal zirconia were identified in all groups and peaks corresponding to the crystalline phase of cubic zirconia were identified only for the 3Y-TZP group. Based on the results of density, flexural strength and microstructure of the material, only the groups sintered at 1400 °C were selected for optical characterization, biological analysis and additional mechanical testing.

3.3. Weibull analysis and optical properties

Table 3 shows the values of characteristic strength (σ_0), Weibull modulus (m) with their respective 95% confidence intervals and the mean, standard deviation and coefficient of variation for L, a and b parameters for all materials sintered at 1400 °C. The strength value for 3Y-TZP (642.4 MPa) was statistically higher than the value obtained for the composite (436.6 MPa). The Weibull modulus of the 3Y-TZP group (5.8) was statistically lower than that of the T12.5 group (10.8). Fig. 4 shows the relationship between fracture probability and fracture stress (Weibull plot) for the two materials evaluated. It was possible to observe that the regression curve of the composite had a lower slope than that of the group 3Y-TZP.

Table 3 indicates that there were significant differences among the values of L, a and b obtained for the two materials tested. The highest values of L and b were obtained for T12.5 and the highest value of a was obtained for the 3Y-TZP. The color difference (ΔE_{00}) between the two materials measured on a white background was 2.23 ± 0.26.

3.4. Probability of failure

Table 4 shows the estimated failure probability for fatigue tests performed under stresses of 50 or 100 MPa and after missions of 1, 3 or 5 million cycles. The probability of failure varied significantly, ranging from 0.04% (3Y-TZP group tested for one million cycles at 50 MPa) to 17.4% (composite group tested for 5 million cycles at 100 MPa). It was possible to observe that under the same conditions (number of cycles and stress level) the T12.5 group always showed a greater probability of failure than the control. Regardless of the material, the probability of failure was higher when there was an increase in the number of cycles or the stress level. In relation to the parameter beta (β) calculated in the Weibull++ software, the 3Y-TZP group showed a value (confidence interval) of 0.38 (0.24–0.61), which was similar to that of the composite group, which showed a value of beta of 0.45 (0.26–0.77).

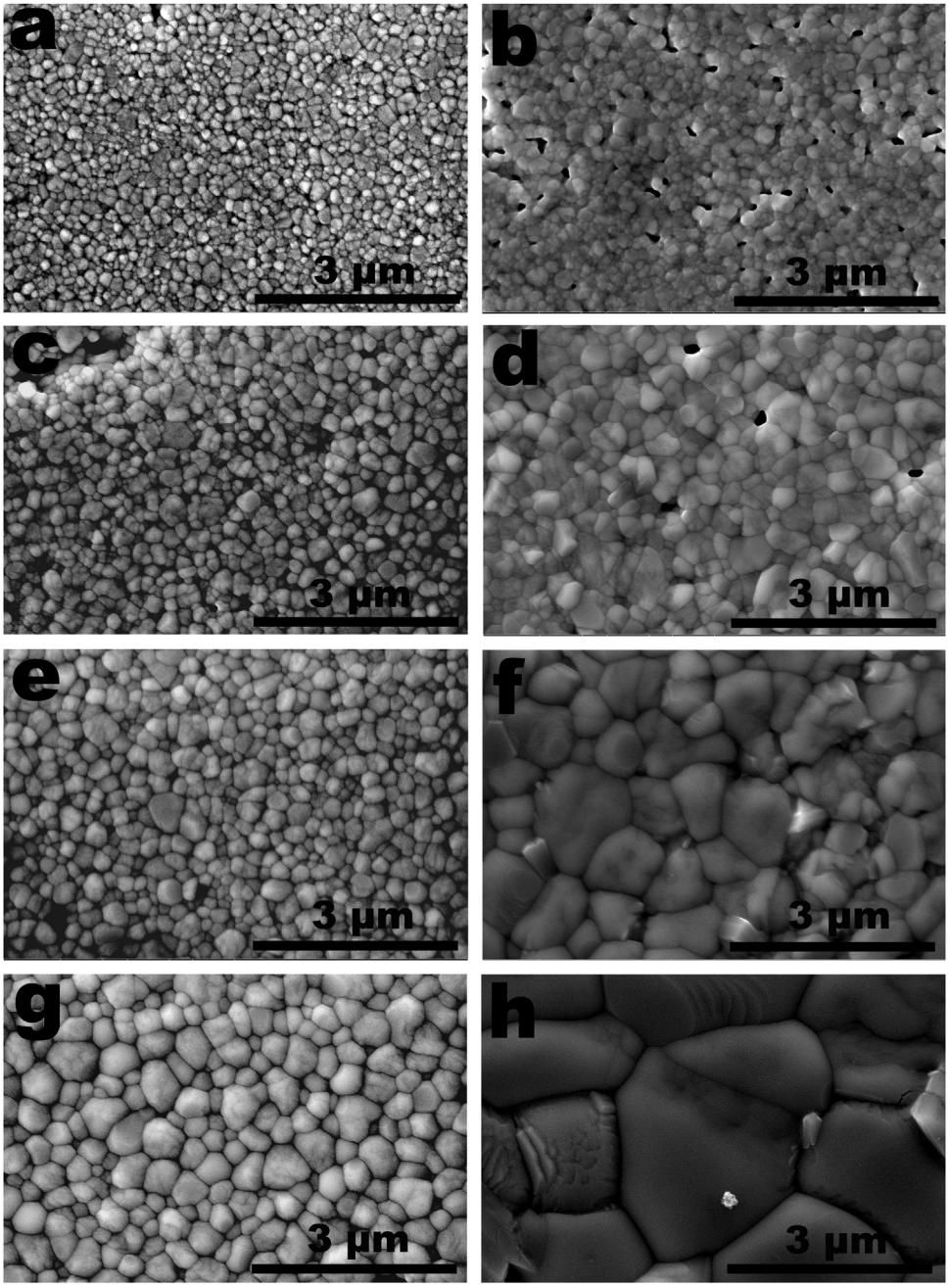

Fig. 1 – Scanning electron micrographs of 3Y-TZP (left) and 3Y-TZP/TiO_2 (right) specimens after polishing and thermally etched. Group 3Y-TZP (a) and 3Y-TZP/TiO_2 (b) sintered at 1200°C/1h. Group 3Y-TZP (c) and 3Y-TZP/TiO_2 (d) sintered at 1300°C/1h. Group 3Y-TZP (e) and 3Y-TZP/TiO_2 (f) sintered at 1400°C/1h. Group 3Y-TZP (g) and 3Y-TZP/TiO_2 (h) sintered at 1500°C/1h.

Table 3 – Characteristic strength (σ_0), Weibull modulus (m) and Beta (β) with their respective 95% confidence intervals and mean ± standard deviation (coefficient of variation) of L, a, b. Values followed by the same letter are statistically similar (p > 0.05).

Material	Characteristic strength, σ_0 (MPa)	Weibull modulus, m	L	A	B
3Y-TZP	642.4[a](598.0–688.9)	5.8[b](4.2–7.8)	92.0[b] ± 0.6 (0.6%)	−1.18[a] ± 0.3 (25%)	3.87[b] ± 0.82 (21%)
T12.5	436.6[b](421.4–451.9)	10.8[a](8.1–14.1)	93.3[a] ± 0.6 (0.6%)	−1.52[b] ± 0.2 (15%)	6.35[a] ± 0.14 (2%)

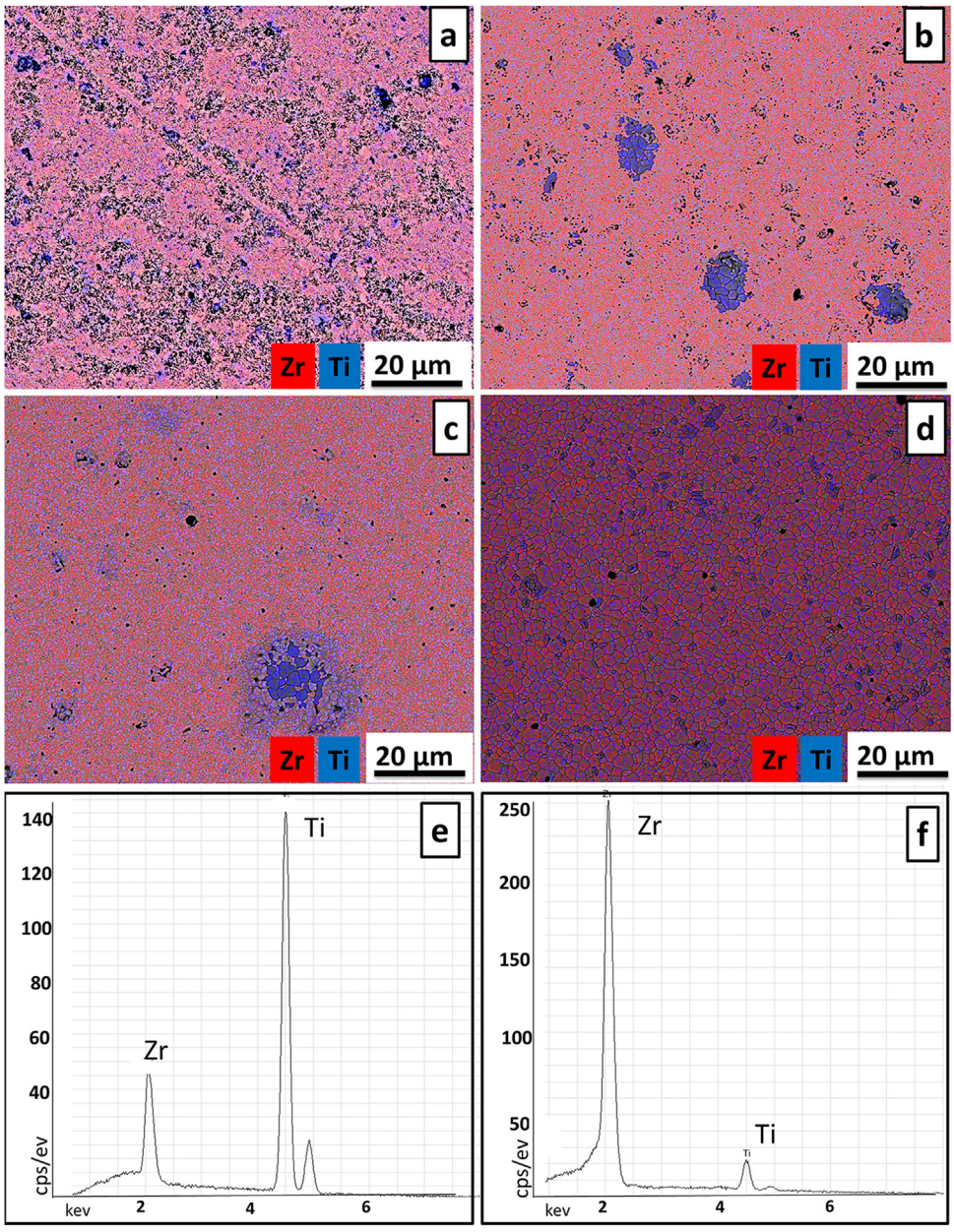

Fig. 2 – Scanning electron micrographs and chemical characterization of 3Y-TZP/TiO_2 specimens by elementary mapping by Energy Dispersive X-ray Spectroscopy (EDS) sintering at different temperatures: 1200°C/1h (a), 1300°C/1h (b), 1400°C/1h (c) and 1500°C/1h (d) and EDS point (e and f).

Table 4 – Probability of failure (%) estimated for fatigue tests performed under a stress of 50 or 100 MPa and after 1, 3 or 5 million cycles.

Material	Stress	Number of cycles		
		1×10^6	3×10^6	5×10^6
3Y-TZP	50 MPa	0.04 (0.005–0.35)	0.06 (0.01–0.52)	0.07 (0.01–0.62)
	100 MPa	0.17 (0.02–1.45)	0.25 (0.03–2.13)	0.31 (0.04–2.57)
T12.5	50 MPa	2.3 (0.6–8.1)	3.7 (0.9–14.1)	4.7 (1.1–18.3)
	100 MPa	8.8 (3.1–23.4)	14.0 (4.5–39.3)	17.4 (5.2–49.2)

3.5. *Biological analysis*

The results of the biological properties of the ceramic materials are illustrated in Figs. 5 and 6. The Osteo-1 cells adhered and spread at the top of both ceramic materials. The cells showed a flat and polygonal shape with multiple cytoplasm processes (lamellipodia) of varying lengths independent of the substrate in which they were grown (Fig. 5).

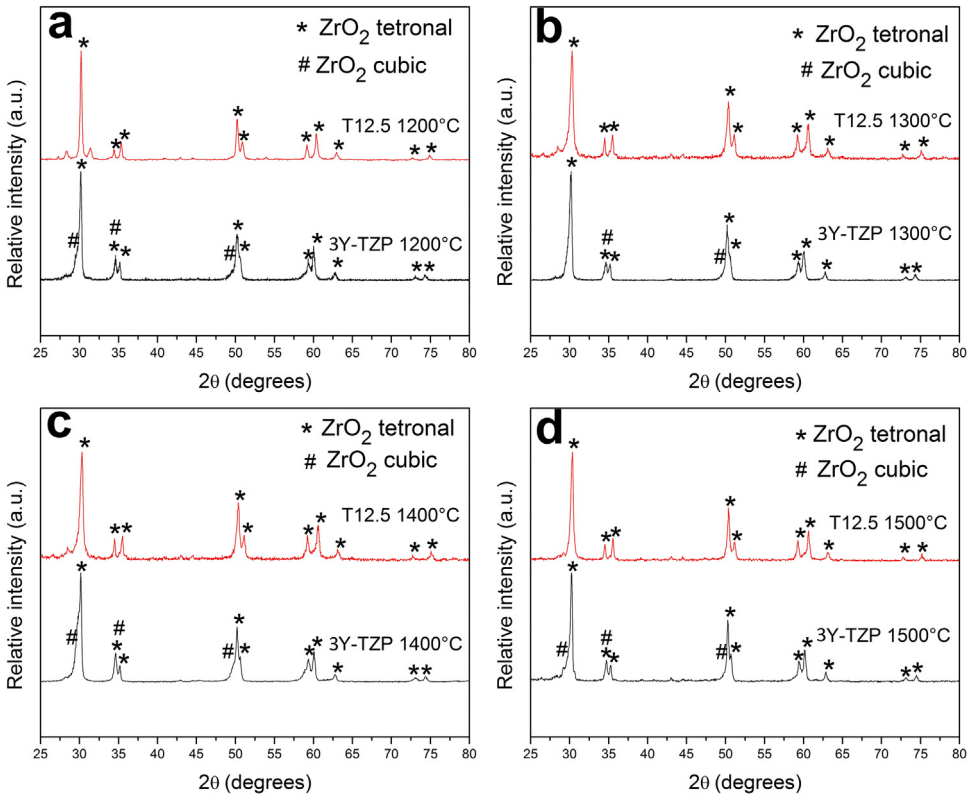

Fig. 3 – X-ray diffraction patterns of 3Y-TZP and 3Y-TZP/TiO_2 pellets sintering at 1200°C/1h (a); 1300°C/1h (b); 1400°C/1h (c) and 1500°C/1h (d).

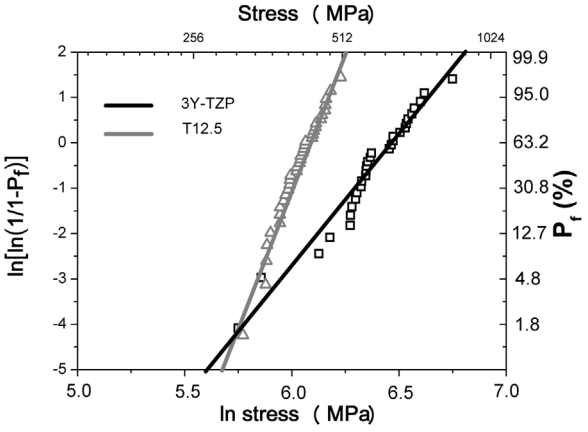

Fig. 4 – Weibull plot showing the failure probability (P_f) as a function of the stress.

Fig. 6a shows graphically the proliferation of Osteo-1 cells of the three experimental groups. There was significant cell growth in all groups during the experimental time. No statistical differences were found between the three groups up to 3 days after plating. After 4 days, it was possible to observe a significantly higher cell proliferation rate for both the T12.5 group and the control group in relation to the 3Y-TZP group. The highest cell viability was observed at the end of the experimental time (6 days) in the T12.5 group. Quantitative results of extracellular matrix mineralization of Osteo-1 cells assayed by Alizarin Red staining is shown in Fig. 6b. The T12.5 group showed significantly higher formation of mineralization nodules than both the positive control and the 3Y-TZP group.

4. Discussion

The results demonstrated the great potential of using the 3Y-TZP/TiO_2 composite as a dental implant material. The developed material did not interfere with osteoblast-like cells adhesion (Fig. 5), but rather favored a greater cell proliferation and functional differentiation (Fig. 6). The new ceramic material showed no perceptible color differences when compared to 3Y-TZP and the predicted probability of failure under fatigue is less than 4.7% after 5 million cycles under tension of 50 MPa (Table 4).

The sintering temperature and the presence of TiO_2 significantly affected the microstructure, density and flexural strength of the 3Y-TZP/TiO_2 composite (Table 2), so the first hypothesis was accepted. In relation to grain size, it is known that Ti has a smaller ionic radius compared the radius of Zr and this allows a greater mobility of the atoms, leading to the formation of larger grains in the 3Y-TZP/TiO_2 composite [28]. Another factor contributing to the increase in grain size is the high sintering temperature, which also facilitates the attraction among particles and consequently increases the densification by means of the elimination of pores [29].

Regarding the microstructure, it is important to note that, although the XRD analysis did not identify the presence of titania or zirconium titanate, the mapping images (Fig. 2) evidenced the presence of regions with high concentrations

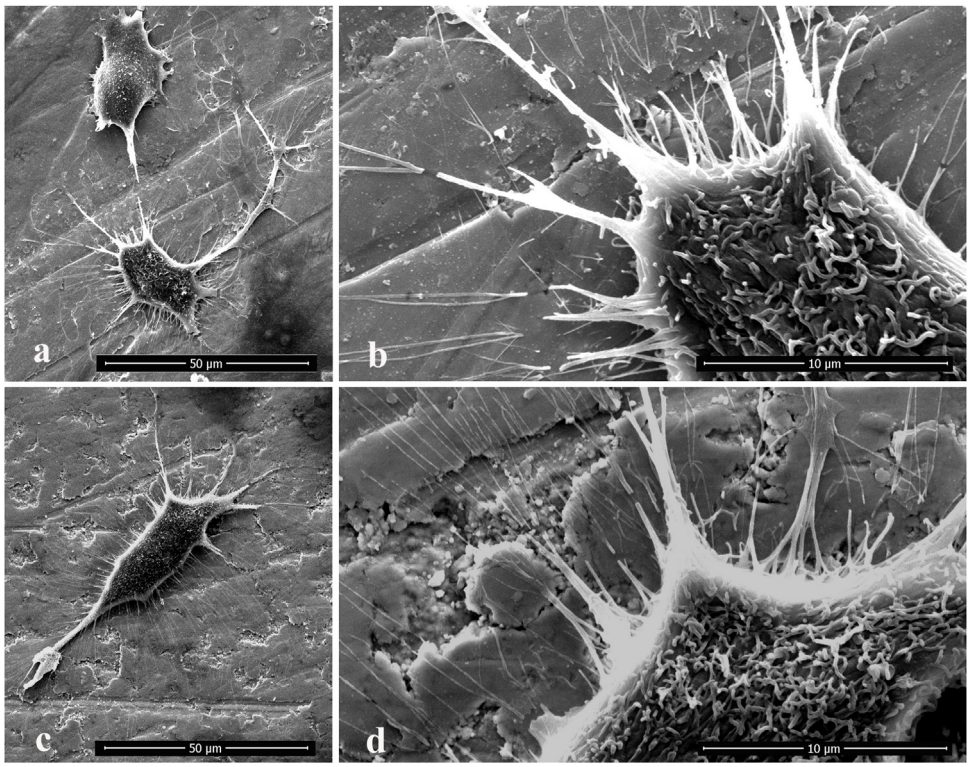

Fig. 5 – Scanning electron microscopy images of Osteo-1 cells on 3Y-TZP (a,b) and T12.5 (c,d). Observe the intimate contact of the cellś lamillipodia with both materials (b,d).

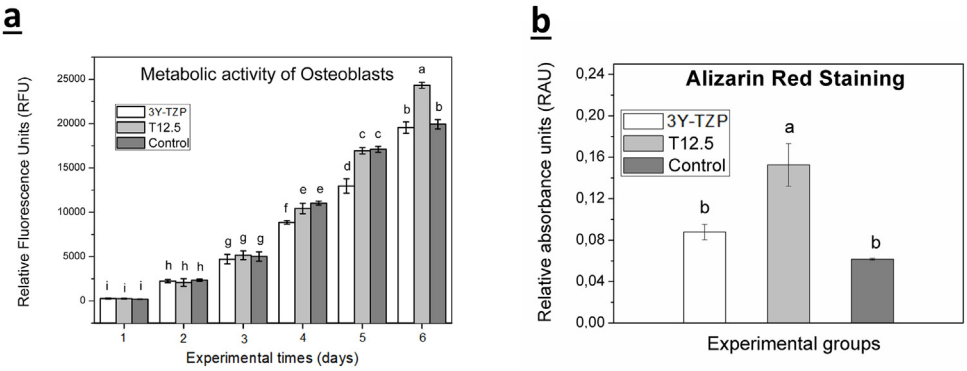

Fig. 6 – Biological responses of Osteo-1 cells to Y-TZP, T12.5 and control. (a) graphic representation of the cell proliferation and (b) differentiation at 21 days. Bars topped by different letters are statistically different ($p \leq 0.05$).

of the chemical element Ti in the composite. These regions correspond to a titaniaum compound and were probably not identified in the diffractograms (Fig. 3) because they are present in a reduced amount and the XRD technique is not sensitive enough in these situations. This means that the major portion of titanium is in solid solution in the zirconia net.

Considering the flexural strength, several studies showed that the addition of titania or other materials to the 3Y-TZP matrices decreases the final mechanical property, since these ceramic materials have lower flexural strength compared to 3Y-TZP [10,11]. One of the main causes for the reduction in strength is the increase in porosity. Pores are important stress concentrators and may become fracture origins [30]. Because of the high porosity, specimens produced with lower sintering temperatures were not used in the second part of this investigation and only specimens sintered at 1400 °C were used for further optical, mechanical and biological characterization.

Most of the studies on 3Y-TZP/TiO_2 composite evaluated the mechanical properties and the microstructure of the material, however none of them evaluated the optical properties [19,21,22,31]. As far as we know, the present investigation was the first one that proposed to perform this type of color analysis in this type of composite. The International Commission on Illumination defined the following parameters: 1) L, brightness, whereby the closer to 100, the brighter the material; 2) a, color coordinate red/green, with positive values indicating red and negative indicating green e 3) b, color coordinate yel-

low/blue, with positive values indicating yellow and negative indicating blue.

The addition of titania to 3Y-TZP caused a slight increase in brightness and a tendency towards a more yellowish and greener color in the ceramic composite. However, the ΔE_{00} between the 3Y-TZP and the T12.5 was less than 2.25, which is the 50% acceptability limit of color change for dental materials [32]. This limit indicates that a trained observer cannot perceive the color difference between 3Y-TZP and T12.5. This can be considered a positive result, since when it comes to the development of a material for aesthetic applications, it is important that the color is not significantly altered with respect to the color of the control (3Y-TZP).

The lower characteristic strength of the T12.5 (Table 3) can be explained by the lower mechanical properties of titania in relation to 3Y-TZP. It is also observed in Table 3 that characteristic strength values for the 3Y-TZP (642 MPa) were relatively lower than those found in the literature (911 MPa) [33]. This may be related to the relatively rough surface finish of the specimens of the present work, which simulates the real surface of dental implants. The lower slope of the regression curve (Fig. 5) on the Weibull plot is a visual representation indicating that the 3Y-TZP/TiO_2 composite has a Weibull modulus significantly higher than that of the 3Y-TZP. Probably this is related to a lower variability in the sizes of defects that can lead to failure of this composite and, therefore, indicates that the T12.5 is a material with greater structural reliability. However, the present work was not able to obtain a 3Y-TZP/TiO_2 composite which, in addition to a larger Weibull modulus, presented values of flexural strength and likelihood of failure similar to those measured for 3Y-TZP. One possible way to optimize the ceramic composite would be by means of more effective pressing techniques and sintering furnaces [34,35].

There is no consensus in the literature regarding the stress levels developed in dental implants and bone tissue. Different studies simulated these stresses with finite element analyses and the results showed a great variation in the stress level from 5 to 600 MPa. Multiple parameters were tested in these studies, such as the design/diameter of the implants and the direction/level of the simulated load [36–39]. Thus, the present study chose to estimate the probability of failure with tensions of 50 MPa or 100 MPa, which were meant to simulate normal chewing and parafunction conditions, respectively. The composite showed a good performance for the lower stress levels (50 MPa), with the fracture probability not exceeding 5% after 5 million cycles, while in parafunctional stress levels, the probability increased to 17.4%.

It is important to emphasize that clinical reality involves many other factors such as: a) the environment in which the implant is placed is a mixture of saliva, blood and bone; b) the population of defects present on the surface of the implant can be altered during insertion; c) the impact that the implant undergoes during chewing; d) the existence of oblique and horizontal loads; e) bulk failure of dental implants, either clinically or in the laboratory, occurs from the root of the first exposed thread. All of these factors may contribute to the fact that the probability of clinical failure is even greater than those shown in the present study.

The calculated value of beta is related to a change in the failure rate during the test. Values of beta greater than 1.0 indicate that the failure rate is increasing with time, and therefore, there is damage accumulation during testing [25]. Thus, factors related to cycling (number of cycles, applied load and frequency) and coarse finishing of the pellets may explain the low beta values for the two groups in the present study.

In addition to the optical and mechanical properties, the success of an implant involves a good osseointegration and therefore it is fundamental the presence of appropriate adhesion, cellular proliferation and functional differentiation represented by the formation of mineralized extracellular matrix on the material surface. In the case of dental implants, the cells involved in these processes are the osteoblasts. The advantages of using the osteoblast cell culture in implant research are the isolated and homogeneous nature of the osteoblast system, a defined temporal course of events, the reproducible growth of multiple cultures, relatively limited expense and the reduced animal morbidity and mortality. One limitation of this type of study is that the bulk implant substrates are opaque and not amenable to transmitted light microscopy [40]. Thus, we used SEM to be able to observe the morphology and the distribution of the Osteo-1 cells on the top of both ceramic materials. In the SEM as well as in the first periods of the cell proliferation assay (e.g., up to 4 days) it was observed that addition of titania to Y-TZP did not interfere with cell adhesion; however, the effects of this addition led to relevant improvement on progressive cell proliferation and on their functional differentiation, which is of paramount importance for osseointegration. During whole experimental time the T12.5 group showed cell proliferation similar that that of positive control, where the osteoblasts were grown in the best cell culture conditions. Moreover, 4 days after seeding (Fig. 6), the T12.5 and control cells showed higher cell proliferation compared to 3Y-TZP. This illustrates the already described lack of bioactivity of the 3Y-TZP [8], drawback of this ceramic that was circumvented by the addition of titania, as T12.5 demonstrated a bioactivity improving the cell division, even reaching the highest viability at the end of the experimental time. Moreover, after 21 days in culture, the T12.5 was able to induce the osteoblasts to produce mineralized nodules at a higher amount than the positive controls and also higher than the 3Y-TZP group. This result was of paramount importance, since for the Alizarin red assay the cells were grown under clonogenic medium, and no mineralizing medium was used, condition that would impair the mineralization of the extracellular matrix for the lack in ions in the culture medium. Then, for mineralizing the synthesized extracellular matrix, the cells of the T12.5 group certainly used the ions released from this ceramic in a higher extent than the 3Y-TZP group. A previous work has already shown this tendency [16] and the literature associates titania to better adhesion, spreading, proliferation, cell differentiation and the formation of hydroxyapatite [14,15,17].

A possible explanation for this phenomenon would be that the water molecules are adsorbed on the surface of the titania and consequently form the groups Ti−OH. Hydroxyl groups (−OH) are related to protein adsorption and cellular behavior [41]. Molecular simulations show that hydroxyl groups can bind to the $-COO^-$ and $-NH_3^+$ groups present in proteins by means of hydrogen bonds [42]. Thus, the presence of titania favors the binding of proteins such as fibronectin, which pro-

vides even more binding sites for the cells, leading to better cell adhesion and proliferation in the 3Y-TZP/TiO_2 composite when compared to 3Y-TZP [12]. Therefore, the second hypothesis tested was not accepted, since the 3Y-TZP group and the T12.5 group showed different behavior in relation to the evaluated parameters: optical properties, characteristic strength (σ_o), Weibull modulus (m), fatigue behavior and proliferation and production of nodules of mineralization by osteoblasts.

5. Conclusion

The lower sintering temperatures (1200 and 1300 °C) reduced the density, strength and grain size of both the 3Y-TZP and T12.5. The addition of titania in 12.5 wt% decreased the density, flexural strength and increased the grain size of the composite in relation to the 3Y-TZP. The sintering temperature of 1400 °C was the most appropriate for sintering both the 3Y-TZP and the composite. The composite developed have good aesthetic properties, as it presents no perceptible color change when compared to 3Y-TZP and showed enhanced proliferation rate and production of mineralized nodules on its surface when compared to 3Y-TZP. However, its microstructure and mechanical properties need to be improved for future dental implant applications.

Acknowledgement

This work was supported by Fundação de Amparo à Pesquisa do Estado de São Paulo - FAPESP - Grant # 2017-11913-8.

REFERENCES

[1] Larsson C, Wennerberg A. The clinical success of zirconia-based crowns: a systematic review. Int J Prosthodont 2014;27:33–43, http://dx.doi.org/10.11607/ijp.3647.

[2] Kniha K, Schlegel KA, Kniha H, Modabber A, Hölzle F, Kniha K. Evaluation of peri-implant bone levels and soft tissue dimensions around zirconia implants—a three-year follow-up study. Int J Oral Maxillofac Surg 2018;47:492–8, http://dx.doi.org/10.1016/j.ijom.2017.10.013.

[3] Stout MM, Cook BK, Arola DD, Fong H, Raigrodski AJ, Bollen AM. Assessing the feasibility of yttria-stabilized zirconia in novel designs as mandibular anterior fixed lingual retention after orthodontic treatment. Am J Orthod Dentofacial Orthop 2017;151:63–73, http://dx.doi.org/10.1016/j.ajodo.2016.04.032.

[4] Chevalier J, Gremillard L, Virkar AV, Clarke DR. The tetragonal-monoclinic transformation in zirconia: lessons learned and future trends. J Am Ceram Soc 2009;92:1901–20, http://dx.doi.org/10.1111/j.1551-2916.2009.03278.x.

[5] Garvie RC, Hannink RH, Pascoe RT. ©1975 Nature Publishing Group. Nature 1975;258:703–4.

[6] Cao Y, Yu C, Wu Y, Li L, Li C. Long-term survival and peri-implant health of titanium implants with zirconia abutments: a systematic review and meta-analysis. J Prosthodont 2019;28:883–92, http://dx.doi.org/10.1111/jopr.13097.

[7] Kniha K, Kniha H, Grunert I, Edelhoff D, Hölzle F, Modabber A. Esthetic evaluation of maxillary single-tooth zirconia implants in the esthetic zone. Int J Periodontics Restorative Dent 2019;39:e195–201, http://dx.doi.org/10.11607/prd.3282.

[8] Treccani L, Yvonne Klein T, Meder F, Pardun K, Rezwan K. Functionalized ceramics for biomedical, biotechnological and environmental applications. Acta Biomater 2013;9:7115–50, http://dx.doi.org/10.1016/j.actbio.2013.03.036.

[9] Matsumato TJ, An SH, Ishimoto T, Nakano T, Matsumoto T, Imazato S. Zirconia-hydroxyapatite composite material with micro porous structure. Dent Mater 2011;27:e205–12, http://dx.doi.org/10.1016/j.dental.2011.07.009.

[10] Bicalho LA, Baptista CARP, Souza RC, Santos C, Strecker K, Barboza MJR. Fatigue and subcritical crack growth in ZrO_2-bioglass ceramics. Ceram Int 2013;39:2405–14, http://dx.doi.org/10.1016/j.ceramint.2012.08.093.

[11] Miranda RB de P, Miranda WG, Lazar DRR, Ussui V, Marchi J, Cesar PF. Effect of titania content and biomimetic coating on the mechanical properties of the Y-TZP/TiO_2 composite. Dent Mater 2018;34:238–45, http://dx.doi.org/10.1016/j.dental.2017.11.003.

[12] Hong Y, Yu M, Lin J, Cheng K, Weng W, Wang H. Surface hydroxyl groups direct cellular response on amorphous and anatase TiO_2 nanodots. Colloids Surf B Biointerfaces 2014;123:68–74, http://dx.doi.org/10.1016/j.colsurfb.2014.08.030.

[13] Uchida M, Kim HM, Kokubo T, Fujibayashi S, Nakamura T. Structural dependence of apatite formation on titania gels in a simulated body fluid. J Biomed Mater Res A 2003;64:164–70, http://dx.doi.org/10.1002/jbm.a.10414.

[14] Yu WQ, Jiang XQ, Zhang FQ, Xu L. The effect of anatase TiO_2 nanotube layers on MC3T3-E1 preosteoblast adhesion, proliferation, and differentiation. J Biomed Mater Res A 2010;94:1012–22, http://dx.doi.org/10.1002/jbm.a.32687.

[15] He J, Zhou W, Zhou X, Zhong X, Zhang X, Wan P, et al. The anatase phase of nanotopography titania plays an important role on osteoblast cell morphology and proliferation. J Mater Sci Mater Med 2008;19:3465–72, http://dx.doi.org/10.1007/s10856-008-3505-3.

[16] Marchi J, Ussui V, Delfino CS, Bressiani AHA, Marques MM. Analysis in vitro of the cytotoxicity of potential implant materials. I: zirconia-titania sintered ceramics. J Biomed Mater Res B Appl Biomater 2010;94:305–11, http://dx.doi.org/10.1002/jbm.b.31652.

[17] Wang N, Li H, Lü W, Li J, Wang J, Zhang Z, et al. Effects of TiO_2 nanotubes with different diameters on gene expression and osseointegration of implants in minipigs. Biomaterials 2011;32:6900–11, http://dx.doi.org/10.1016/j.biomaterials.2011.06.023.

[18] Ussui V, Leitao F, Yamagata C, Menezes CAB, Lazar DRR, Paschoal JOA. Synthesis of ZrO_2-based ceramics for applications in SOFC. Mater Sci Forum 2003;416–418:681–6, http://dx.doi.org/10.4028/www.scientific.net/msf.416-418.681.

[19] Zeng XM, Du Z, Schuh CA, Tamura N, Gan CL. Microstructure, crystallization and shape memory behavior of titania and yttria co-doped zirconia. J Eur Ceram Soc 2016;36:1277–83, http://dx.doi.org/10.1016/j.jeurceramsoc.2015.11.042.

[20] Marchi J, Amorim EM, Lazar DRR, Ussui V, Bressiani AHA, Cesar PF. Physico-chemical characterization of zirconia-titania composites coated with an apatite layer for dental implants. Dent Mater 2013;29:954–62, http://dx.doi.org/10.1016/j.dental.2013.07.002.

[21] Hodgson SNB, Cawley J. The effect of titanium oxide additions on the properties and behaviour of Y-TZP. J Mater Process Technol 2001;119:112–6, http://dx.doi.org/10.1016/S0924-0136(01)00885-8.

[22] Miao X, Sun D, Hoo PW, Liu J, Hu Y, Chen Y. Effect of titania addition on yttria-stabilised tetragonal zirconia ceramics sintered at high temperatures. Ceram Int 2004;30:1041–7, http://dx.doi.org/10.1016/j.ceramint.2003.10.025.

[23] ISO-6872. Dentistry-ceramic materials. ISO-6872; 2015, n.d.
[24] ISO/TR 28642, n.d. Technical Report(E): Dentistry - Guidance on colour measurements; 2016.
[25] Bonfante EA, Coelho PG. A critical perspective on mechanical testing of implants and prostheses. Adv Dent Res 2016;28:18–27, http://dx.doi.org/10.1177/0022034515624445.
[26] Lavos-Valereto I de C, Deboni MCZ, Azambuja N, Marques MM. Evaluation of the titanium Ti-6Al-7Nb alloy with and without plasma-sprayed hydroxyapatite coating on growth and viability of cultured osteoblast-like cells. J Periodontol 2002;73:900–5, http://dx.doi.org/10.1902/jop.2002.73.8.900.
[27] Togashi AY, Cirano FR, Marques MM, Pustiglioni FE, De Lima LAPA. Characterization of bone cells obtained from the calvaria of neonatal rats (osteo-1) after serial subculture. J Appl Oral Sci 2007;15:442–7, http://dx.doi.org/10.1590/S1678-77572007000500013.
[28] Hwang S-L, Chen I-W. Grain size control of tetragonal zirconia polycrystals using the space charge concept. J Am Ceram Soc 1990;73:3269–77, http://dx.doi.org/10.1111/j.1151-2916.1990.tb06449.x.
[29] Lupulescu A, Glicksman ME. Diffusion-limited crystal growth in silicate systems: similarity with high-pressure liquid-phase sintering. J Cryst Growth 2000;211:49–61, http://dx.doi.org/10.1016/S0022-0248(99)00841-6.
[30] Yoshimura HN, Molisani AL, Narita NE, Cesar PF, Goldenstein H. Porosity dependence of elastic constants in aluminum nitride ceramics. Mater Res 2007;10:127–33, http://dx.doi.org/10.1590/S1516-14392007000200006.
[31] Miao X, Sun D, Hoo PW. Effect of Y-TZP addition on the microstructure and properties of titania-based composites. Ceram Int 2009;35:281–8, http://dx.doi.org/10.1016/j.ceramint.2007.10.017.
[32] Ghinea R, Pérez MM, Herrera LJ, Rivas MJ, Yebra A, Paravina RD. Color difference thresholds in dental ceramics. J Dent 2010;38:57–64, http://dx.doi.org/10.1016/j.jdent.2010.07.008.
[33] Borba M, De Araújo MD, Fukushima KA, Yoshimura HN, Cesar PF, et al. Effect of the microstructure on the lifetime of dental ceramics. Dent Mater 2011;27:710–21, http://dx.doi.org/10.1016/j.dental.2011.04.003.
[34] Flamant Q, Caravaca C, Meille S, Gremillard L, Chevalier J, Biotteau-Deheuvels K, et al. Selective etching of injection molded zirconia-toughened alumina: Towards osseointegrated and antibacterial ceramic implants. Acta Biomater 2016;46:308–22, http://dx.doi.org/10.1016/j.actbio.2016.09.017.
[35] Toshihiko I, Shinya H, Hideshi S, Hodaka S, Yasutomo Y, Masao Y. Influence of surface treatment of yttria-stabilized tetragonal zirconia polycrystal with hot isostatic pressing on cyclic fatigue strength. Dent Mater J 2013;32:274–80, http://dx.doi.org/10.4012/dmj.2012-247.
[36] Iranmanesh P, Abedian A, Nasri N, Ghasemi E, Khazaei S. Stress analysis of different prosthesis materials in implant-supported fixed dental prosthesis using 3D finite element method. Dent Hypotheses 2014;5:109–14, http://dx.doi.org/10.4103/2155-8213.136757.
[37] de Moraes SLD, Verri FR, Santiago Júnior JF, Almeida DA de F, et al. Three-dimensional finite element analysis of varying diameter and connection type in implants with high crown-implant ratio. Braz Dent J 2018;29:36–42, http://dx.doi.org/10.1590/0103-6440201801746.
[38] Kumar Ga, Kovoor L, Oommen V. Three-dimensional finite element analysis of the stress distribution around the implant and tooth in tooth implant-supported fixed prosthesis designs. J Dent Implant 2011;1:75, http://dx.doi.org/10.4103/0974-6781.91283.
[39] Lofaj F, Kucera J, Nemeth D, Kvetkova L. Finite element analysis of stress distributions in mono- and bi-cortical dental implants. Mater Sci Eng C 2015;50:85–96, http://dx.doi.org/10.1016/j.msec.2015.01.095.
[40] Cooper LF, Masuda T, Yliheikkilä PK, Felton DA. Generalizations regarding the process and phenomenon of osseointegration. Part II. in vitro studies. Int J Oral Maxillofac Implants 1998;13:163–74.
[41] Roach P, Farrar D, Perry CC. Interpretation of protein adsorption: surface-induced conformational changes. J Am Chem Soc 2005;127:8168–73, http://dx.doi.org/10.1021/ja042898o.
[42] Shen JW, Wu T, Wang Q, Pan HH. Molecular simulation of protein adsorption and desorption on hydroxyapatite surfaces. Biomaterials 2008;29:513–32, http://dx.doi.org/10.1016/j.biomaterials.2007.10.016.